Supplementary Information (SI) for Journal of Materials Chemistry A.
This journal is © The Royal Society of Chemistry 2024

Supporting information for "Polymorphism Control of Fast-sintered NASICON-type $LiZr_2(PO_4)_3$"

Lin Lin† and Kelsey B. Hatzell*,†,‡

†*Andlinger Center for Energy and the Environment, Princeton University, Princeton, NJ 08540, USA*

‡*Department of Mechanical and Aerospace Engineering, Princeton University, Princeton, NJ 08540, USA*

E-mail: kelsey.hatzell@princeton.edu

Details of modified air-compatible UHS experiments

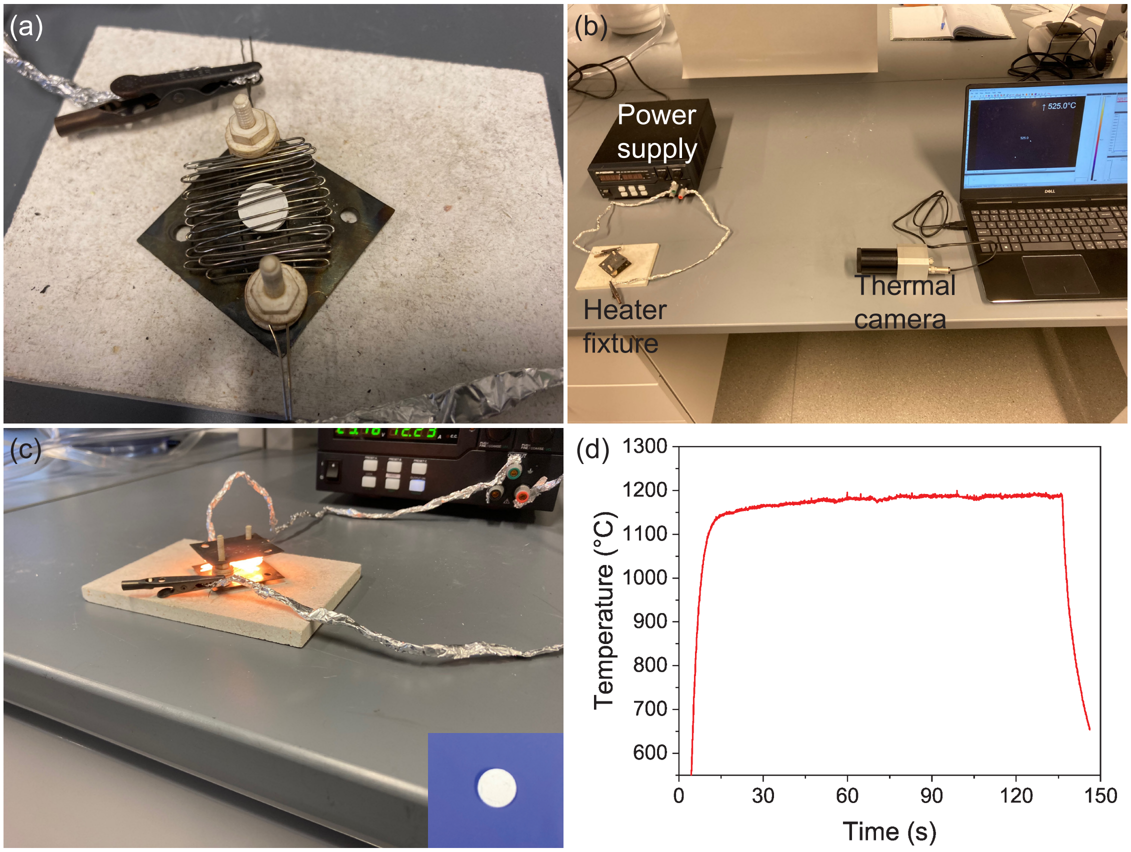

Figure S1: (a) Photograph of the home-made air-compatible UHS setup, with a pressed green body pellet sitting between kanthal heating elements (top heat shielding piece is removed). (b) Photograph of the experimental setup with the heater fixture described in (a) with a set of alloy heat shielding, power supply, thermal camera, and a laptop computer recording the temperature profile. (c) Photograph of the heater fixture under operation, with heating elements glowing. Bottom-right corner - a polished LZP pellet sintered by UHS for 5 min. (d) Temperature-time plot on a sample of a UHS experiment, showing rapid heating and cooling as well as short dwelling time.

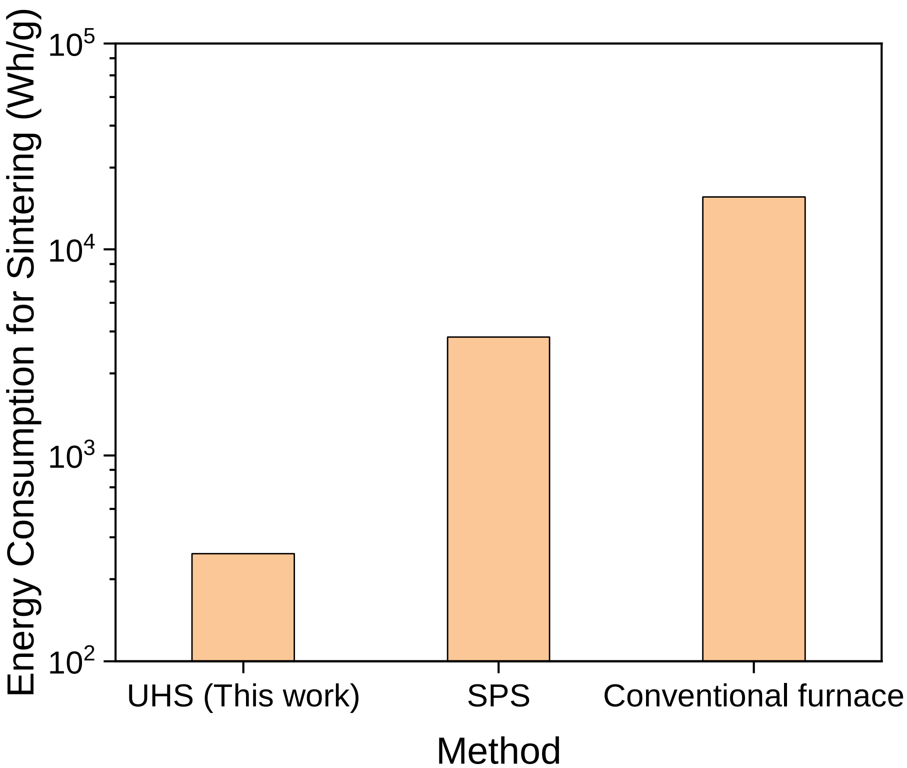

Figure S2: Comparison on energy consumption for sintering unit mass of LiZr2(PO4)3 ceramics among the air-compatible ultrafast sintering employed in this work, typical spark plasma sintering (SPS) employed in references,[1,2] and conventional furnace sintering employed in.[3] Order-of-magnitude smaller energy consumption per unit mass is demonstrated in the UHS method employed in this work.

EDS measurement of polished pellet

Table S1: Elemental percentages of a polished UHS LZP pellet, measured with SEM-based EDS. The elemental ratios of Zr:O:P (2.07:2.18:1) agrees with the ideal stoichiometry (1.96:2.07:1). The signals of C and Si come from the SiC polishing paper and organic solvents used for polishing. The Li signal is not detectable by EDS because of the limitation of the detector. There is no Al, Cr or Fe signal detected, suggesting the atoms in the kanthal heating elements do not significantly diffuse into the LZP pellets.

Element	Weight percentage	Standard deviation
Zr	33.6	1.3
O	35.3	0.8
P	16.2	0.6
C	11.8	0.4
Si	3.0	0.2

Rietveld Refinement Results

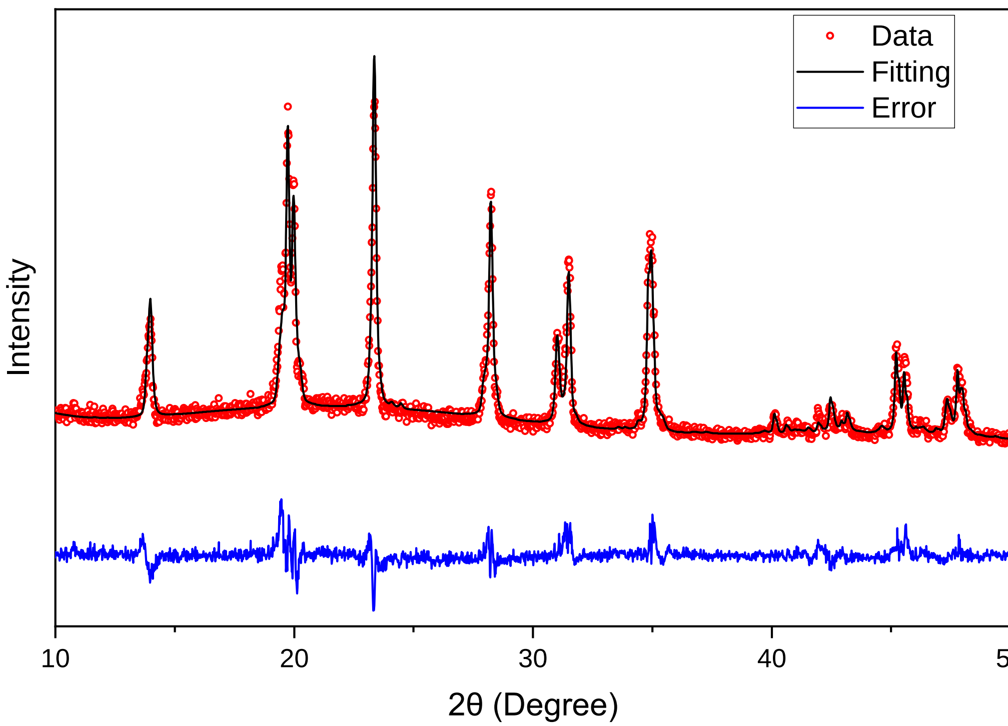

Figure S3: Rietveld refinement results and error for XRD data on 2-min sintered pellet from fine powders. Fitting parameters: R_p=0.417, R_{wp}=0.328, chi^2=2.93.

Table S2: Refined lattice parameters for the two phases.

Phase	Space Group	a (Å)	b (Å)	c (Å)	α (°)	β (°)	γ (°)
Rhombohedral	$R\bar{3}c$	8.8635	8.8635	22.0993	90	90	120
Triclinic	$C\bar{1}$	15.1643	8.8391	9.1497	89.7309	124.2842	90.4958

Dependence of polymorphism on sintering time

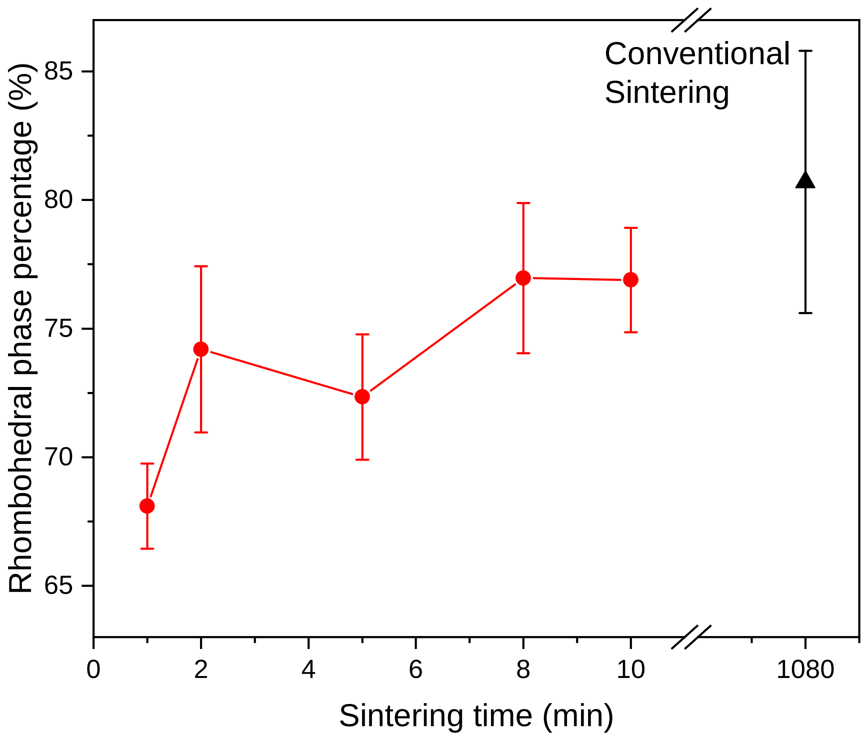

Figure S4: Rhombohedral phase ratio calculated from Rietveld refinement, as a function of sintering time, suggesting the ratio a stable value of 75% with sintering longer than 2 min. The 1080 min datapoint is from a pellet conventionally sintered at 1200 °C for 18 h.

Dependence of polymorphism on sample depth towards surface

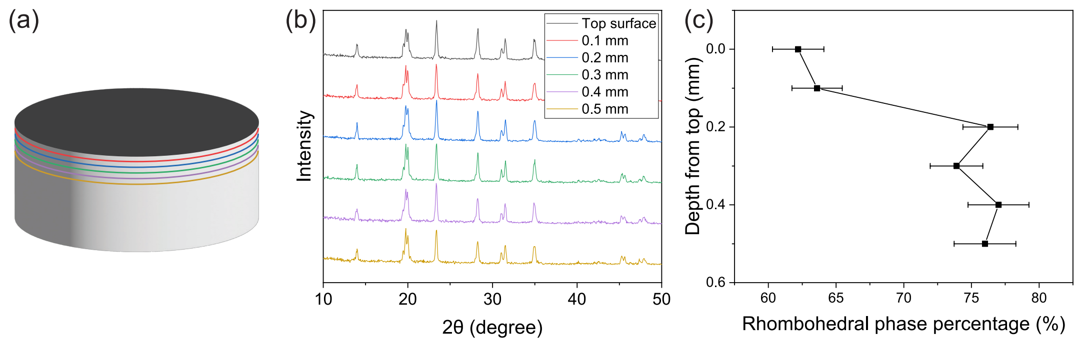

Figure S5: Rhombohedral phase ratio as a function of depth towards the top surface obtained by polishing off the top regions of pellets until different depths. (a) Schematic illustration of the locations with different depth towards the surface. (b) XRD data for different depths. (c) Rhombohedral ratio of different depths calculated from Rietveld refinement. The ratio gets to a stable 75% value after polishing off by more than 0.2 mm.

Intial polymorphism of green body

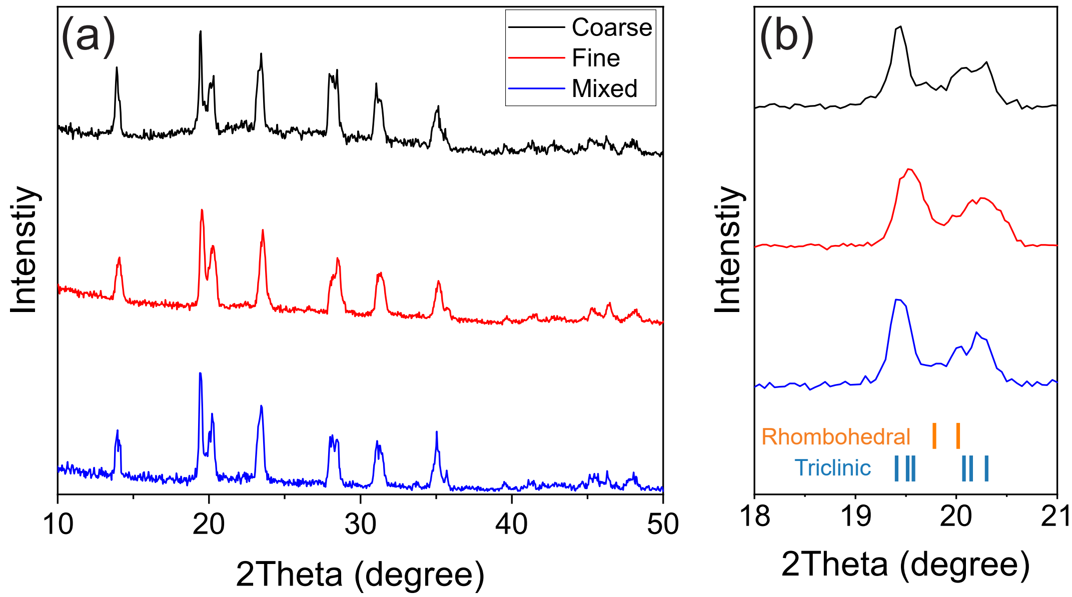

Figure S6: XRD results (a) and zoom-in scans for powders with different particle sizes. All of them demonstrate predominantly triclinic phase.

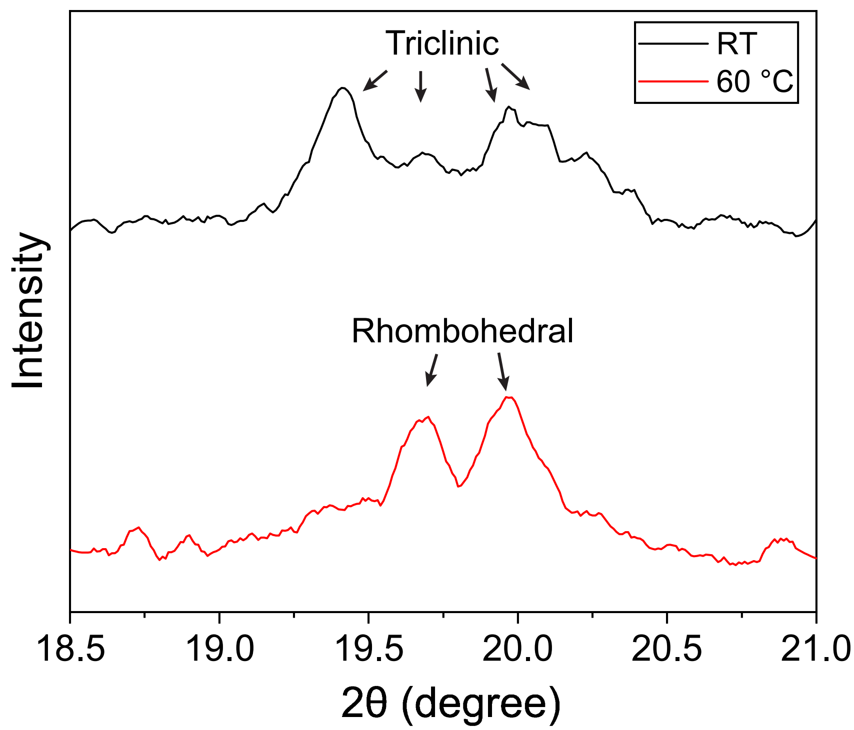

Figure S7: Zoom-in XRD scans between $2\theta = 18.5^\circ$ to 21° for a green-body pellet at room temperature and 60 °C. The more splitted peaks in the sample at room temperature corresponds to a nearly pure triclinic phase, whereas a pure rhombohedral phase is observed when it is heated up to 60 °C.

LZP Polymorphism impact on transport and electrochemistry

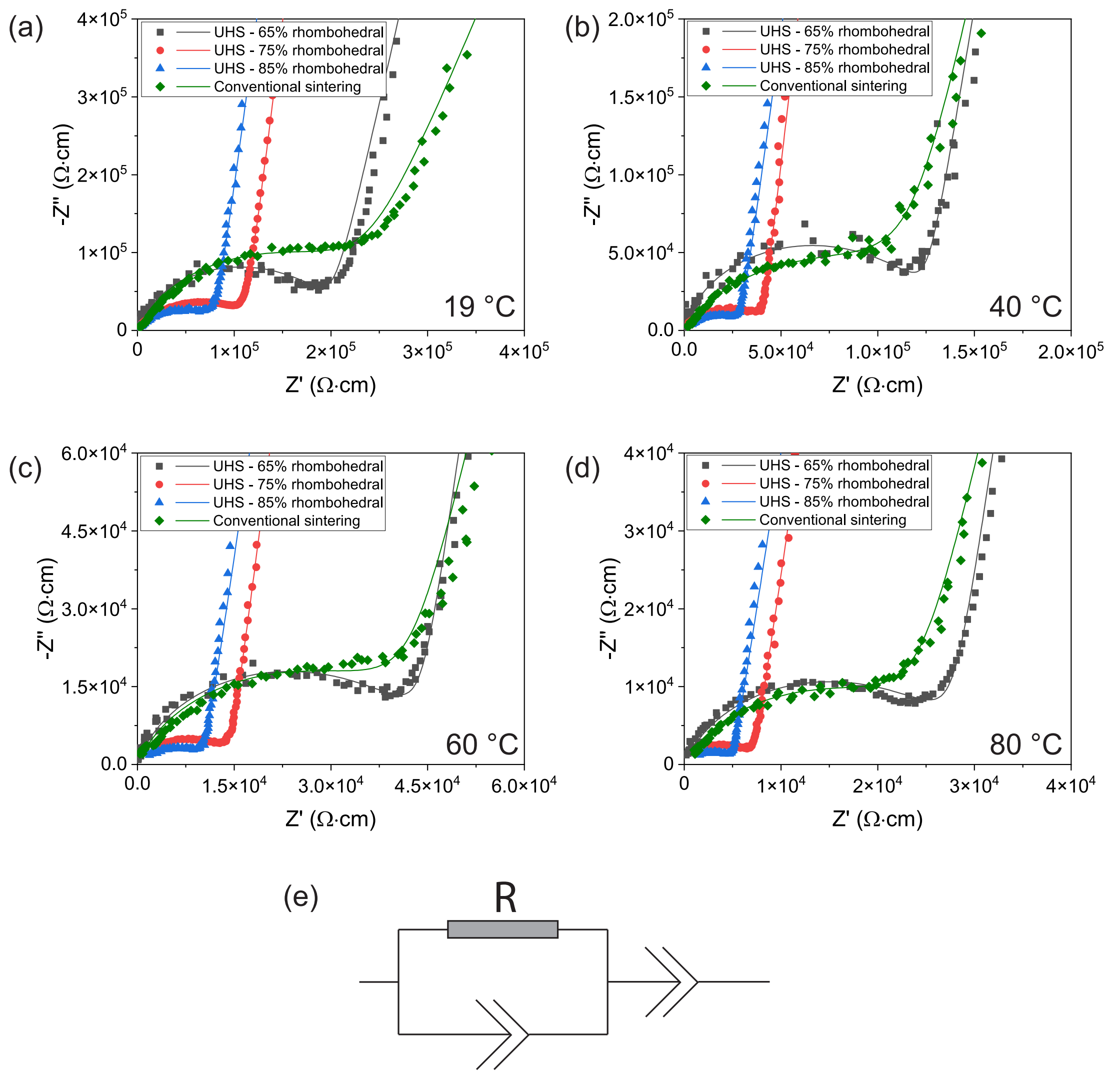

Figure S8: Electrochemical impedance spectroscopy of LZP pellets prepared by UHS as well as conventional sintering, with 65% sample prepared by sintering a pellet pressed from coarse powders for 2 min, 75% sample by sintering a pellet from fine powders for 2 min, and 85% sample by sintering a green body with sintering aid. (a)-(d) Electrochemical impedance spectroscopy of samples at (a) room temperature, (b) 40 °C (c) 60 °C, (d) 80 °C. (e) The Equivalent circuit for fitting the EIS plots.

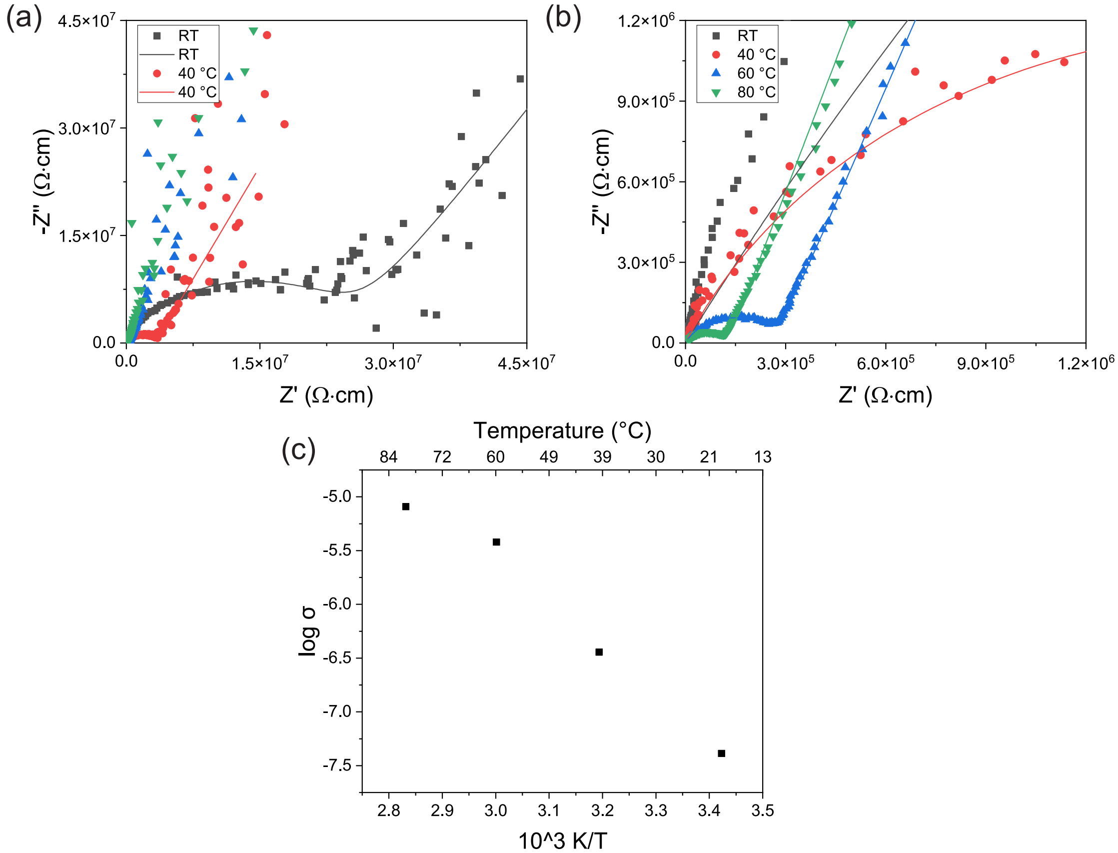

Figure S9: (a) Electrochemical impedance spectroscopy of the sample sintered from mixed powders for 2 min. (b) Zoomed-in plot of (a). (c) The dependence of ionic conductivity on temperature.

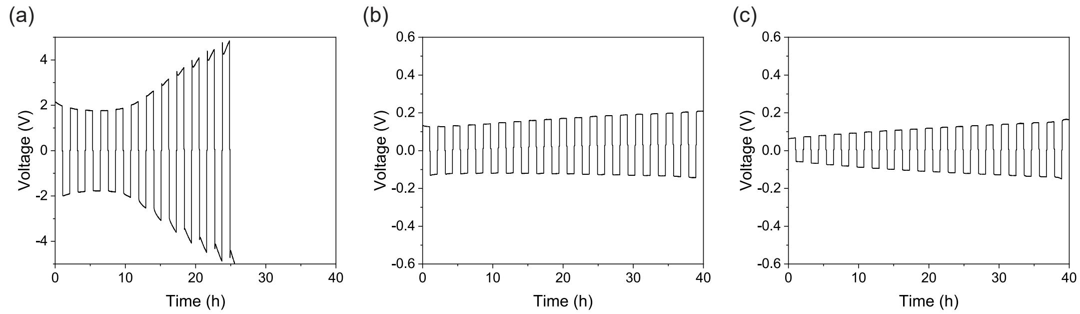

Figure S10: Cycling stability data for pellets with (a)65%, (b) 75% and (c)85% of rhombohedral phases. Compared to 75% and 85% rhombohedral samples, 65% show significant voltage increase.

References

(1) Li, Y.; Zhou, W.; Chen, X.; Lü, X.; Cui, Z.; Xin, S.; Xue, L.; Jia, Q.; Goodenough, J. B. Mastering the interface for advanced all-solid-state lithium rechargeable batteries. *Proceedings of the National Academy of Sciences* **2016**, *113*, 13313–13317.

(2) Loutati, A.; Odenwald, P.; Aktekin, B.; Sann, J.; Guillon, O.; Tietz, F.; Fattakhova-Rohlfing, D. Survey of Zirconium-Containing NaSICON-type Solid-State Li+ Ion Conductors with the Aim of Increasing Reduction Stability by Partial Cation Substitution. *Batteries & Supercaps* **2022**, *5*, e202200327.

(3) Catti, M.; Stramare, S.; Ibberson, R. Lithium location in NASICON-type Li+ conductors by neutron diffraction. I. Triclinic α-LiZr2 (PO4) 3. *Solid State Ionics* **1999**, *123*, 173–180.